PHYSICAL REVIEW E **91**, 031104(R) (2015)

Direct observation of the two-plasmon-decay common plasma wave using ultraviolet Thomson scattering

R. K. Follett,[1,2,*] D. H. Edgell,[1] R. J. Henchen,[1] S. X. Hu,[1] J. Katz,[1] D. T. Michel,[1] J. F. Myatt,[1] J. Shaw,[1] and D. H. Froula[1,2]

[1]*Laboratory for Laser Energetics, University of Rochester, 250 East River Road, Rochester, New York 14623, USA*

[2]*Department of Physics and Astronomy, University of Rochester, Rochester, New York 14623, USA*

(Received 19 December 2014; published 26 March 2015)

A 263-nm Thomson-scattering beam was used to directly probe two-plasmon-decay (TPD) excited electron plasma waves (EPWs) driven by between two and five 351-nm beams on the OMEGA Laser System. The amplitude of these waves was nearly independent of the number of drive beams at constant overlapped intensity, showing that the observed EPWs are common to the multiple beams. In an experimental configuration where the Thomson-scattering diagnostic was not wave matched to the common TPD EPWs, a broad spectrum of TPD-driven EPWs was observed, indicative of nonlinear effects associated with TPD saturation. Electron plasma waves corresponding to Langmuir decay of TPD EPWs were observed in both Thomson-scattering spectra, suggesting the Langmuir decay instability as a TPD saturation mechanism. Simulated Thomson-scattering spectra from three-dimensional numerical solutions of the extended Zakharov equations of TPD are in excellent agreement with the experimental spectra and verify the presence of the Langmuir decay instability.

DOI: 10.1103/PhysRevE.91.031104 PACS number(s): 52.35.Fp, 52.35.Mw, 52.35.Qz, 52.38.Kd

The self-organization of nonlinearly interacting dynamic systems into coherent synchronized states has attracted a broad interest across a range of subject areas in the biological and physical sciences [1]. Within plasma physics, multiple-beam laser facilities provide the opportunity for synchronization of parametric instabilities driven by intense laser beams propagating through long-scale-length plasma. The recent activation of the 192 beam National Ignition Facility has brought multiple-beam laser-plasma instabilities to the forefront, and understanding the origin of these instabilities is one of the most significant hurdles preventing the realization of inertial confinement fusion (ICF) [2,3]. Although progress has been made in understanding the coupling of multiple beams to ion-acoustic waves (IAWs) [4], other multibeam instabilities are not well understood.

Two-plasmon decay (TPD) is a three-wave parametric instability in which an electromagnetic wave decays into two electron plasma waves (EPWs) [5], and when multiple laser beams are used, their interactions with EPWs can be synchronized by phase coupling to common decay waves [6]. The resulting large-amplitude EPWs can stochastically accelerate electrons from the bulk velocity distribution to high energies (>30 keV) [7,8]. In ICF implosions, these high-energy electrons preheat the cold fuel, degrading implosion performance, and potentially preventing ignition [9]. Numerical simulations predict that once the TPD instability is driven above the linear threshold, EPW amplitudes rapidly reach levels where secondary processes such as the Langmuir decay instability (LDI) [10] and cavitation lead to a broad spectrum of large-amplitude EPWs [11–13].

Early multiple-beam experiments showed evidence of TPD-generated hot electrons when the single-beam growth rates were significantly below threshold. These studies suggested that TPD hot-electron generation was governed by the overlapped laser intensity [14]; subsequent experiments showed that hot-electron generation scaled with the maximum multiple-beam growth rate calculated from linear theory [15]. These studies used indirect measurements of TPD, dependent on nonlinear processes associated with generating a broad TPD spectrum, which challenges the validity of comparing to linear TPD theory. Self-Thomson scattering of the drive laser beams provides a more direct signature of TPD-driven EPWs [16,17], and the spectral features have been discussed in theoretical studies of TPD-driven LDI [18], but quantitative comparison was limited by the difficulty in defining the EPWs that are probed when using large numbers of drive beams [19,20]. Very early laser-plasma experiments made the most direct experimental observations of TPD by using a Thomson-scattering probe to observe the amplitude, which is proportional to the square root of the scattered power, and frequency of EPWs driven by a single CO_2 laser [21–23].

This Rapid Communication presents direct observation of two-plasmon-decay waves driven by multiple laser beams and the TPD-driven Langmuir decay instability. An ultraviolet Thomson-scattering probe beam was used to isolate EPWs driven by multiple-beam TPD, which allowed for a quantitative comparison of numerical simulations of TPD with experiments. The narrow width [1.6 ± 0.1 nm full width at half maximum (FWHM)] and peak wavelength (423.1 ± 0.2 nm) of the common-wave scattering feature shows that the electron plasma waves are driven near the region of maximum common-wave growth. A second peak in the scattering spectrum, corresponding to Langmuir decay of primary TPD EPWs, suggests the Langmuir decay instability as a TPD saturation mechanism. The measured Thomson-scattering spectra were well reproduced by three-dimensional (3D) numerical simulations that account for the nonlinear nature of the instability and the multiple-beam geometry used in the experiments.

The experiments were conducted on the OMEGA Laser Facility [24] and used two to five $\lambda_{3\omega} = 351$ nm laser beams to drive common EPWs. The beam ports were on five of the corners of a hexagon, with the beams incident on a planar target

*rfollett@lle.rochester.edu

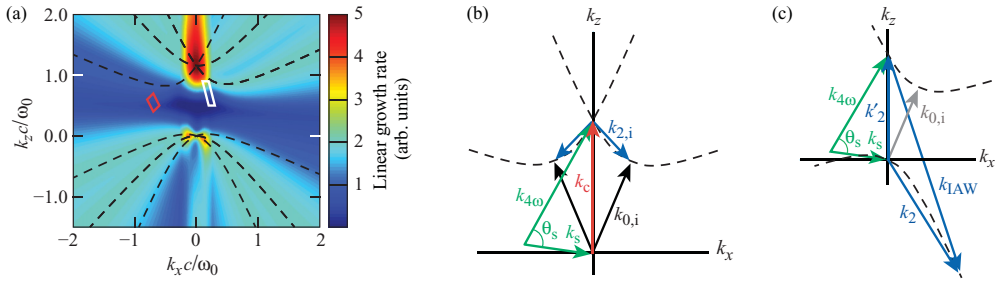

FIG. 1. (Color online) (a) The normalized five-beam common-wave growth rate (color scale) in the Thomson-scattering plane [defined by $\hat{y}||(\hat{k}_{4\omega} \times \hat{k}_s)$ with the target normal in the $-\hat{z}$ direction] showing that the five-beam common-wave matching conditions are satisfied only along the z axis. The dashed curves show the linear TPD theory maximum growth for each drive beam. The range of wave vectors probed in the two Thomson diagnostic configurations, common-wave geometry (white box) and non-common-wave geometry (red box). (b) Wave-matching conditions for Thomson scattering ($\mathbf{k}_c = \mathbf{k}_{4\omega} - \mathbf{k}_s$) from common TPD EPWs, and (c) daughter EPWs from Langmuir decay of backscattered TPD EPWs ($\mathbf{k}'_2 = \mathbf{k}_2 - \mathbf{k}_{iaw} = \mathbf{k}_{4\omega} - \mathbf{k}_s$).

at an angle of 23° with respect to the target normal. Phase plates [25] were used on each beam to define the 300-μm FWHM flat-top laser spots at best focus of the $f/6.7$ focusing lenses. To improve the uniformity of the laser beam profile, the beams propagated through a birefringent polarization smoothing crystal that separated the incident linearly polarized laser beam into two overlapped beams with orthogonal polarizations propagating at a slight angle (~40 μrad) [26]. The laser beams used 1- or 2-ns-long square pulses with the same energy in each beam. When the number of beams and pulse lengths were varied, the laser energies were adjusted to maintain a constant vacuum overlapped intensity (~10^{15} W/cm^2), resulting in the same hydrodynamic conditions for all experiments. The planar targets were 3 mm × 3 mm squares consisting of 30-μm-thick CH layers coated on 30-μm-thick Mo. The CH-layer thickness was chosen such that the burnthrough time was much longer than the laser pulse [27].

The Thomson-scattering diagnostic consisted of a $\lambda_{4\omega} = 263.25$ nm $f/6.7$ probe beam with a best-focus diameter of ~50 μm [28]. The probe beam used the same pulse shape and duration as the drive beams with ~70 J of total energy (intensity ~10^{15} W/cm^2). The Thomson-scattered light was collected by a reflective $f/10$ collection system coupled to two spectrometer/streak cameras, used to simultaneously observe the EPW and IAW scattering features [29]. The spectral resolutions of the IAW and EPW systems are 0.05 and 0.5 nm, respectively. Scattered light was collected from an ~50 × 50 × 50 μm^3 volume located either 150 μm ($n_e/n_c \approx 0.18$–0.21) or 100 μm ($n_e/n_c \approx 0.21$–0.25) from the target surface (where n_e is the electron density and $n_c = 9.05 \times 10^{21}$ cm^{-3} is the critical density for 351-nm light). The angle between the collection optic and probe beam was 120°. Two Thomson-scattering geometries were used to probe EPW wave vectors near the region of maximum common-wave growth (common-wave configuration) and a region where there was no linear common-wave coupling (non-common-wave configuration). The range of wave vectors probed in the two configurations [Fig. 1(a)] was calculated by ray tracing through density profiles generated using the two-dimensional (2D) hydrodynamic code DRACO, where the electron heat flux was limited to 6% of the free-streaming value [30]. Refraction reduced the scattering angle in the plasma to $\theta_s^{cw} \approx 32°$ and $\theta_s^{ncw} \approx 55°$ in the common-wave and non-common-wave configurations, respectively.

Two-plasmon-decay linear theory with multiple laser beams predicts a maximum growth rate along the axis of symmetry defined by the laser beams [the z axis in Fig. 1(a)] [6]. The frequency ($\omega_0 = \omega_1 + \omega_2$) and wave vector ($\mathbf{k}_0 = \mathbf{k}_1 + \mathbf{k}_2$) matching conditions and linear EPW dispersion relation ($\omega_{1,2}^2 = \omega_{pe}^2 + 3k_{1,2}^2 v_{te}^2$) can be satisfied for multiple beams sharing a common daughter wave only when they share a common angle relative to the driven wave [where ($\omega_{1,2}$,$\mathbf{k}_{1,2}$) are the daughter EPW frequencies and wave vectors, (ω_0,$\mathbf{k}_0$) are the drive beam frequency and wave vector, $\omega_{pe} = \omega_0\sqrt{n_e/n_c}$ is the electron plasma frequency, and $v_{te} = \sqrt{T_e/m_e}$ is the electron thermal velocity (m_e is the electron mass)].

In experiments where multiple beams share a common azimuthal angle, the maximum linear growth rate occurs at the intersection of the single-beam maximum growth rates, which lie along hyperboloids [$k_\perp = k_{||}(k_{||} - k_0)$, where $k_\perp$ and $k_{||}$ are the components of the plasma wave vector perpendicular and parallel to the drive beam wave vector, respectively] [15]. The hexagonal beam pattern has reflection symmetry with respect to the Thomson-scattering plane, resulting in only three unique intersections of the single-beam maximum growth hyperboloids with the Thomson-scattering plane [giving six lines (one for each hyperboloid branch) in Fig. 1(a)]. Electron plasma waves corresponding to distinct branches of a hyperboloid are categorized as forward scattered ($\omega_1 > \omega_0/2$, $\mathbf{k}_1 \cdot \mathbf{k}_0 > 0$) or backscattered ($\omega_2 < \omega_0/2$,$\mathbf{k}_2 \cdot \mathbf{k}_0 < 0$). Figure 1(b) shows the wave vector-matching condition for Thomson scattering from forward-scattered common TPD EPWs, $\mathbf{k}_c = \mathbf{k}_{4\omega} - \mathbf{k}_s$ (where $\mathbf{k}_{4\omega}$,$\mathbf{k}_s$, and $\mathbf{k}_c$ are the wave vectors of the probe beam, Thomson-scattered light, and common EPW, respectively). The associated matching conditions and dispersion relations [31] constitute a closed set of equations and predict a Thomson-scattered peak wavelength of $\lambda_{s,c} = 423 \pm 0.5$ nm.

Figure 2(a) shows a broad (9.1 ± 1.1 nm FWHM) EPW Thomson-scattering spectrum measured 150 μm from the initial target surface. The scattering feature has a single spectral peak with a shape consistent with the size and intensity distribution of the probe beam, indicating that thermal

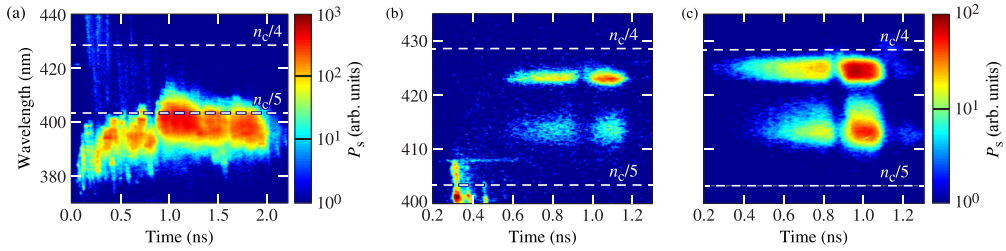

FIG. 2. (Color online) Thomson-scattering spectra for scattering from EPWs with dashed lines at wavelengths corresponding to the quarter ($n_c/4$) and fifth ($n_c/5$) critical surfaces. (a) Scattering from thermal EPWs (150 μm from the target surface) generates a broad spectrum corresponding to the range of densities within the Thomson-scattering volume. (b) Scattering spectra from common EPWs (100 μm from the target surface) shows narrow peaks corresponding to locally driven TPD EPWs. (c) Off-hyperbola scattering (100 μm from the target surface) results in a broad spectrum of TPD-driven EPWs. The dip in scattering amplitude at 0.9 ns in all three spectra is caused by a shock [32], reflected from the molybdenum layer, traveling through the Thomson-scattering volume.

EPWs of roughly equal amplitudes are present throughout the (physical) scattering volume. The observed peak corresponds to Thomson scattering from EPWs from a range of densities $n_e/n_c \approx 0.18$–0.21. The IAW spectrum (not shown) was fit to the collisionless dynamic structure factor [33], giving a measure of the electron temperature ($T_e = 2.0 \pm 0.2$ keV at 1 ns) and plasma flow velocity along the target normal ($v_f = 5.5 \pm 0.5 \times 10^7$ cm/s). The predicted values of $T_e = 1.9$ keV and $v_f = 5 \times 10^7$ cm/s from DRACO simulations agree with the measurements.

Figure 2(b) shows a narrow (1.6 ± 0.1 nm FWHM) high-intensity feature that appears at a wavelength ($\lambda_s = 423.1 \pm 0.2$ nm) consistent with the common-wave model ($\lambda_{s,c} = 423 \pm 0.5$ nm). The peak is an order of magnitude more intense and ~10 times narrower than the thermal peak, showing the driven nature of the waves. The wavelength range corresponds to Thomson scattering from densities between $n_e/n_c \approx 0.246$ and 0.247. This is much narrower than the range of densities in the scattering volume ($n_e/n_c \approx 0.21$–0.25), indicating that the peak corresponds to locally driven EPWs.

The integrated Thomson-scattered power in the common-wave configuration (proportional to the square root of the wave amplitude) was nearly independent of the number of drive beams when maintaining a constant overlapped intensity. For two-, three-, and five-beam experiments, the relative Thomson scattered power scaled by 1, 0.7, and 0.5, respectively. The fact that the amplitude of the observed EPWs was nearly independent of the single-beam intensity when varying the number of beams at constant overlapped intensity shows that multiple beams are driving the observed EPWs.

The shorter-wavelength peak ($\lambda_s = 413.7 \pm 0.2$ nm) shown in Fig. 2(b) corresponds to Thomson scattering from EPWs generated by Langmuir decay of backscattered TPD EPWs. Figure 1(c) shows the wave-matching condition for Thomson scattering from secondary backscattered EPWs ($\mathbf{k}_2'$), where the blue triangle satisfies the LDI matching conditions ($\mathbf{k}_2 = \mathbf{k}_2' + \mathbf{k}_{iaw}, \omega_2 = \omega_2' + \omega_{iaw}$). Assuming that the observed EPWs correspond to direct LDI backscatter ($k_2 = k_{iaw} - k_2'$), the matching conditions and dispersion relations [31] give $\lambda_s = 413.8 \pm 0.3$ nm for Thomson scattering from secondary backscattered EPWs, in agreement with the observed peak.

Figure 3(a) compares the measured [Fig. 2(b)] and simulated Thomson-scattering spectra from the five-beam common-wave geometry. The simulated peak widths and amplitude ratio are in excellent agreement with the experiment. The simulation parameters were taken from DRACO profiles: $T_e = 1.9$ keV, $I_{n_c/4} = 6 \times 10^{14}$ W/cm^2, $L_n = 190$ μm (density scale length), $T_i = 1$ keV, $v_{flow} = 5.15 \times 10^7$ cm/s, and $n_e(z) = n_0[1 - (z/L_n)^{1.12}]$, where $n_e(z)$ is a power law fit to the unperturbed electron density profile near $n_c/4$, and $n_0 = 0.27 n_c$ is the peak electron density in the simulation box.

The spectra were simulated using a 3D numerical plasma fluid code (LPSE [34]) that solves the extended Zakharov equations of TPD [18,35] for the low-frequency IAWs and high-frequency (enveloped) EPWs. The Zakharov equations are used to model the nonlinear coupling between EPWs and IAWs [8]. Phase plates with polarization smoothing were simulated by splitting each incident beam cone into two sets of 100 cross-polarized plane-wave beamlets with a 40-μrad angular divergence and random phase. The simulation box was $66 \times 13 \times 13$ μm^3 on a uniform $1300 \times 256 \times 256$ Cartesian grid. Thomson-scattering spectra are generated using a numerical structure factor obtained from simulated time series.

In LPSE simulations, the shorter-wavelength Thomson-scattering peak was correlated to the Langmuir decay of backscattered TPD EPWs by comparing the temporal evolution of the Thomson-scattering spectrum and the low-frequency density perturbations (IAWs). Figure 4(a) shows the simulated EPW spectrum at 1 ps, when the TPD instability was in the linear growth stage, and large-amplitude EPWs

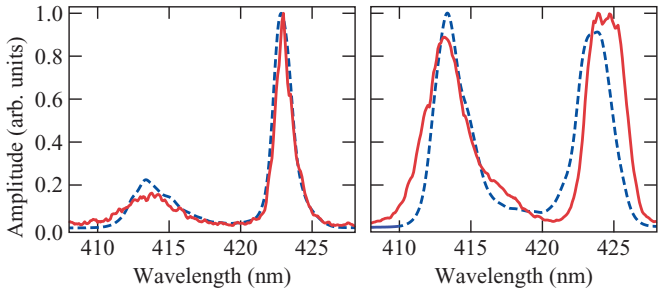

FIG. 3. (Color online) Thomson-scattering spectrum measured at ~1 ns (solid) and simulated (dashed) in the (a) common-wave and (b) non-common-wave Thomson-scattering configurations.

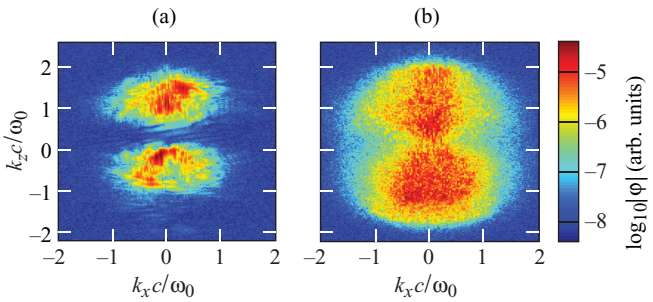

FIG. 4. (Color online) Simulated electron plasma wave spectra for five drive beams (a) during linear TPD growth (1 ps) and (b) after saturation (2 ps), where φ is the high-frequency (enveloped) potential.

corresponding to the maximum five-beam common-wave growth rate are the dominant spectral feature. At this time, the corresponding IAW spectrum has no driven waves, and only the peak corresponding to forward-scattered TPD EPWs is observed in the simulated Thomson-scattering spectrum. When the ponderomotive force associated with the electric field of counterpropagating EPWs is sufficient to overcome IAW damping, a series of Langmuir decays generate large-amplitude IAWs, leading to the broad spectrum of TPD-driven EPWs shown in Fig. 4(b). At this time (∼2 ps), the simulated EPW Thomson-scattering spectrum shows two spectral peaks at wavelengths corresponding to forward- and backscattered TPD EPWs.

In simulations where the intensity was just above the threshold for the onset of the TPD instability ($I_{n_c/4} = 2 \times 10^{14}$ W/cm^2), the EPW amplitudes did not reach sufficient amplitudes to drive large-amplitude IAWs, and the EPW spectrum looks similar to Fig. 4(a) at all times. The spectral peak corresponding to backscattered TPD EPWs does not appear in the low-intensity simulated Thomson-scattering spectra, consistent with these EPWs being generated by LDI.

Figure 2(c) shows a Thomson-scattering spectrum measured in the non-common-wave geometry [red box in Fig. 1(a)], which was chosen such that the Thomson-scattering diagnostic probes wave vectors that do not satisfy the common-wave matching conditions but is measuring light scattered from a range of densities ($n_e/n_c \approx 0.21$–0.25), where TPD is active. The simulated spectrum [Fig. 3(b)] is in good agreement with the measured peak widths and relative amplitudes. The small discrepancy observed between the simulated and measured peak wavelengths could be a result of a ∼10% underestimation of the electron temperature or an overestimation of the effects of refraction. For a given scattering geometry (i.e., fixed θ_s), the location of the peaks is determined by the electron temperature and their separation is approximately linear in electron temperature.

In summary, common TPD EPWs were observed using ultraviolet Thomson scattering. The common-wave Thomson scattering feature is characterized by its narrow width and weak amplitude scaling with overlapped drive beam intensity. The observation of EPWs driven by LDI experimentally shows the nonlinear state of the TPD instability and suggests that LDI is responsible for generating a broad range of plasma wave vectors. These results are supported by 3D LPSE simulations that quantitatively reproduce the experimental Thomson-scattering spectra. The quantitative agreement between these measurements and the modeling will have a significant impact on understanding hot-electron production at large multiple-beam laser facilities that are currently conducting fusion experiments.

We thank D. D. Meyerhofer for useful comments on this manuscript. This material is based upon work supported by the Department of Energy National Nuclear Security Administration under Award No. DE-NA0001944, the University of Rochester, and the New York State Energy Research and Development Authority.

[1] A. Pikovsky, M. Rosenblum, and J. Kurths, *Synchronization: A Universal Concept in Nonlinear Sciences* (Cambridge University Press, Cambridge, UK, 2001).

[2] S. H. Glenzer, B. J. MacGowan, P. Michel, N. B. Meezan, L. J. Suter, S. N. Dixit, J. L. Kline, G. A. Kyrala, D. K. Bradley, D. A. Callahan *et al.*, Science **327**, 1228 (2010).

[3] V. A. Smalyuk, R. Betti, J. A. Delettrez, V. Y. Glebov, D. D. Meyerhofer, P. B. Radha, S. P. Regan, T. C. Sangster, J. Sanz, W. Seka *et al.*, Phys. Rev. Lett. **104**, 165002 (2010).

[4] P. Michel, L. Divol, E. A. Williams, S. Weber, C. A. Thomas, D. A. Callahan, S. W. Haan, J. D. Salmonson, S. Dixit, D. E. Hinkel *et al.*, Phys. Rev. Lett. **102**, 025004 (2009).

[5] E. A. Jackson, Phys. Rev. **153**, 235 (1967).

[6] D. T. Michel, A. V. Maximov, R. W. Short, S. X. Hu, J. F. Myatt, W. Seka, A. A. Solodov, B. Yaakobi, and D. H. Froula, Phys. Rev. Lett. **109**, 155007 (2012).

[7] R. Yan, C. Ren, J. Li, A. V. Maximov, W. B. Mori, Z. M. Sheng, and F. S. Tsung, Phys. Rev. Lett. **108**, 175002 (2012).

[8] J. F. Myatt, H. X. Vu, D. F. DuBois, D. A. Russell, J. Zhang, R. W. Short, and A. V. Maximov, Phys. Plasmas **20**, 052705 (2013).

[9] R. L. McCrory, D. D. Meyerhofer, R. Betti, R. S. Craxton, J. A. Delettrez, D. H. Edgell, V. Y. Glebov, V. N. Goncharov, D. R. Harding, D. W. Jacobs-Perkins *et al.*, Phys. Plasmas **15**, 055503 (2008).

[10] D. F. Dubois and M. V. Goldman, Phys. Rev. **164**, 207 (1967).

[11] H. X. Vu, D. F. DuBois, D. A. Russell, and J. F. Myatt, Phys. Plasmas **17**, 072701 (2010).

[12] J. Meyer and Y. Zhu, Phys. Rev. Lett. **71**, 2915 (1993).

[13] J. Zhang, J. F. Myatt, R. W. Short, A. V. Maximov, H. X. Vu, D. F. DuBois, and D. A. Russell, Phys. Rev. Lett. **113**, 105001 (2014).

[14] C. Stoeckl, R. E. Bahr, B. Yaakobi, W. Seka, S. P. Regan, R. S. Craxton, J. A. Delettrez, R. W. Short, J. Myatt, A. V. Maximov *et al.*, Phys. Rev. Lett. **90**, 235002 (2003).

[15] D. T. Michel, A. V. Maximov, R. W. Short, J. A. Delettrez, D. Edgell, S. X. Hu, I. V. Igumenshchev, J. F. Myatt,

A. A. Solodov, C. Stoeckl *et al.*, Phys. Plasmas **20**, 055703 (2013).

[16] W. Seka, J. F. Myatt, R. W. Short, D. H. Froula, J. Katz, V. N. Goncharov, and I. V. Igumenshchev, Phys. Rev. Lett. **112**, 145001 (2014).

[17] P. E. Young, B. F. Lasinski, W. L. Kruer, E. A. Williams, K. G. Estabrook, E. M. Campbell, R. P. Drake, and H. A. Baldis, Phys. Rev. Lett. **61**, 2766 (1988).

[18] D. A. Russell and D. F. DuBois, Phys. Rev. Lett. **86**, 428 (2001).

[19] W. Seka, D. H. Edgell, J. F. Myatt, A. V. Maximov, R. W. Short, V. N. Goncharov, and H. A. Baldis, Phys. Plasmas **16**, 052701 (2009).

[20] R. L. Berger and L. V. Powers, Phys. Fluids **28**, 2895 (1985).

[21] J. J. Schuss, T. K. Chu, and L. C. Johnson, Phys. Rev. Lett. **40**, 27 (1978).

[22] H. A. Baldis, J. C. Samson, and P. B. Corkum, Phys. Rev. Lett. **41**, 1719 (1978).

[23] H. A. Baldis and C. J. Walsh, Phys. Fluids **26**, 1364 (1983).

[24] T. R. Boehly, R. S. Craxton, T. H. Hinterman, J. H. Kelly, T. J. Kessler, S. A. Kumpan, S. A. Letzring, R. L. Mccrory, S. F. B. Morse, W. Seka *et al.*, Rev. Sci. Instrum. **66**, 508 (1995).

[25] T. J. Kessler, Y. Lin, J. J. Armstrong, and B. Velazquez, in *Laser Coherence Control: Technology and Applications*, edited by H. T. Powell and T. J. Kessler (SPIE, Bellingham, WA, 1993), Vol. 1870, p. 95.

[26] T. R. Boehly, V. A. Smalyuk, D. D. Meyerhofer, J. P. Knauer, D. K. Bradley, R. S. Craxton, M. J. Guardalben, S. Skupsky, and T. J. Kessler, J. Appl. Phys. **85**, 3444 (1999).

[27] B. Yaakobi, P. Y. Chang, A. Solodov, C. Stoeckl, D. H. Edgell, R. S. Craxton, S. X. Hu, J. F. Myatt, F. J. Marshall, W. Seka *et al.*, Phys. Plasmas **19**, 012704 (2012).

[28] A. J. Mackinnon, S. Shiromizu, G. Antonini, J. Auerbach, K. Haney, D. H. Froula, J. Moody, G. Gregori, C. Constantin, C. Sorce *et al.*, Rev. Sci. Instrum. **75**, 3906 (2004).

[29] J. Katz, R. Boni, C. Sorce, R. Follett, M. J. Shoup III, and D. H. Froula, Rev. Sci. Instrum. **83**, 10E349 (2012).

[30] P. B. Radha, V. N. Goncharov, T. J. B. Collins, J. A. Delettrez, Y. Elbaz, V. Y. Glebov, R. L. Keck, D. E. Keller, J. P. Knauer, J. A. Marozas *et al.*, Phys. Plasmas **12**, 032702 (2005).

[31] W. L. Kruer, *The Physics of Laser Plasma Interactions* (Addison-Wesley, Redwood City, CA, 1988).

[32] D. H. Froula, I. V. Igumenshchev, D. T. Michel, D. H. Edgell, R. Follett, V. Y. Glebov, V. N. Goncharov, J. Kwiatkowski, F. J. Marshall, P. B. Radha *et al.*, Phys. Rev. Lett. **108**, 125003 (2012).

[33] D. H. Froula, S. H. Glenzer, N. C. Luhmann, and J. Sheffield, *Plasma Scattering of Electromagnetic Radiation: Theory and Measurement Techniques*, 2nd ed. (Academic, Burlington, MA, 2011).

[34] J. F. Myatt, J. Shaw, J. Zhang, A. V. Maximov, R. W. Short, W. Seka, D. H. Edgell, D. F. DuBois, D. A. Russell, and H. X. Vu, An investigation of Two-Plasmon-Decay Localization in Spherical Implosion Experiments on OMEGA, BAPS **59**(15), 241 (2014). (Session PO4 1).

[35] D. F. DuBois, D. A. Russell, and H. A. Rose, Phys. Rev. Lett. **74**, 3983 (1995).